

Investigating the Effects of the current density on the properties of Ni-P-La₂O₃ composite coatings

Qingdong Lv¹, Xiuqing Fu^{1,2,*}, Xinxin Chen¹, Jinran Lin¹, and Hongbing Cao¹

¹ College of Engineering, Nanjing Agricultural University, Nanjing 210031, China;

² Key laboratory of Intelligence Agricultural Equipment of Jiangsu Province, Nanjing 210031, China

*E-mail: fuxiuqing@njau.edu.cn

Received: 6 August 2020 / Accepted: 12 September 2020 / Published: 30 September 2020

In the present study, the jet electrodeposition technique is applied to improve the wear resistance, electrochemical corrosion resistance and surface hardness of 45# steel. In order to prepare a certain concentration of La₂O₃ particles in the plating solution, properties of Ni-P-La₂O₃ composite coating are investigated by changing the current density from 16 A/dm² to 48 A/dm². After the experiment, physical characteristics of the workpiece, including the surface morphology, chemical composition, hardness and electrochemical corrosion resistance of the composite are analyzed by SEM, EDS and microhardness measuring instruments. Obtained results show that the best performance of the composite coating can be achieved for the current density of 32 A/dm². In this case, the hardness is 822.83HV_{0.1} and the corresponding minimum and maximum self-etching current densities are 5.61E-7 A·cm² and 1.46E-5A·cm², respectively.

Keywords: Jet electrodeposition; Current density; La₂O₃ particles; Ni-P-La₂O₃ composite coating

1. INTRODUCTION

With rapid industrial developments in recent years, more strict requirements are demanded for mechanical parts to improve their performance in all aspects. However, studies show that existing mechanical parts can no longer meet higher industrial requirements. In order to improve the lifetime and other characteristics of mechanical parts, diverse physical, chemical and other methods are usually applied to process the surface of different parts. Studies show that these methods change the surface microstructure, structure and chemical composition of the surface so that better performance can be achieved compared with the base matrix. With the advent of electrodeposition technology, it has been developed rapidly so that it is applied in various industrial fields [1-4]. Considering the superior properties of Ni-P coating, including high hardness and excellent abrasion and corrosion resistance, it has been adopted as one of the most common coatings in diverse industries [5].

In the spray electrodeposition technique, voltage is applied between the cathode and anode. The anode is in direct contact with the nickel rod, while the cathode is in contact with the workpiece. Meanwhile, the plating solution is sprayed on the cathode and workpiece through the anode nozzle, thereby forming a closed-loop [6, 7]. Compared with the conventional electrodeposition, the jet electrodeposition plating solution circulates and accelerates the ion transmission so that improves the limiting current density, thereby improving the deposition rate greatly. Moreover, as the limit current density in the jet electrodeposition increases, the cathode polarization effect strengthens and the formation rate of crystal nucleus accelerates so that the coating grains are more refined. Under these circumstances, a more uniform and compact coating can be obtained, and the surface abrasion resistance and corrosion resistance greatly improve [8-10]. Under the action of the electric field, a coating layer forms on the composite plate by the co-deposition of one or more insoluble particles with metal ions. The prepared coating inherits advantages of particle and metal, so it has been widely used in the industrial production [12, 13].

Rare-earth elements are widely used elements in the electrodeposition. These elements have excellent characteristics, which optimize the surface of the workpiece during the electrodeposition at a deeper level. More specifically, La_2O_3 is one of the most important compounds of rare-earth elements, which its applications have been steadily increasing during the last few years [14]. It is worth noting that La_2O_3 has good physical and chemical properties and plays an important role in civil and military applications [15, 16]. For instance, La_2O_3 is widely applied in glass, ceramics, catalysts, lasers, heating elements, cathode materials and electrical contacts. Recent studies showed that La_2O_3 , which is slightly soluble in water, deposits on the surface of the workpiece in large quantities during electrodeposition and forms a protective layer. In this regard, the application of La_2O_3 in electroplating has been extensively explored. It was found that adding La_2O_3 into the plating solution can greatly improve the hardness, abrasion resistance and corrosion resistance of the coating [17-19].

In the present study, it is intended to apply current densities to prepare a Ni-P- La_2O_3 plating solution. Then an electrospraying test will be carried out and the workpiece will be analyzed accordingly [20].

2. EXPERIMENT SETUP

2.1 Preparation of the coating

In the present study, the test matrix with a dimension of $25\text{mm} \times 10\text{mm} \times 8\text{mm}$ was made of 45# steel. Moreover, the substrate surface was polished by water sandpapers 320#, 800# and 1500#, respectively. The surface quality of the polished workpiece was measured by a laser confocal microscope until the surface roughness reaches $\leq \text{Ra}0.1$. Then the prepared samples are put into an ultrasonic cleaning device in alcohol. Workpieces were activated through the following steps: oil removal → ultrasonic cleaning → weak activation → ultrasonic cleaning → strong activation → ultrasonic cleaning. The processed workpiece was used as the cathode, while the pure nickel rod was used as the anode. The electric spraying test device is presented in Figure 1. The spindle was equipped with a pure nickel bar, which can realize reciprocating movements. Figure 1 indicates that the workpiece is fixed on the cathode, and a clamp is installed on the cathode and anode to apply voltage. When the power supply was

connected, the spindle began to reciprocate. The plating solution was pumped and sprayed on the workpiece on the anode through the nozzle. The ejected plating solution returns to the sump again through the catheter for reuse and improving the deposition efficiency. The bath temperature is set to 60°C, and the spraying time is 20min. After the test, the water pump shuts off immediately and the spindle is closed. Then the workpiece is put in the ultrasonic cleaner for 3 minutes, followed by a blow-dry. Chemical composition of the bath is shown in Table 1.

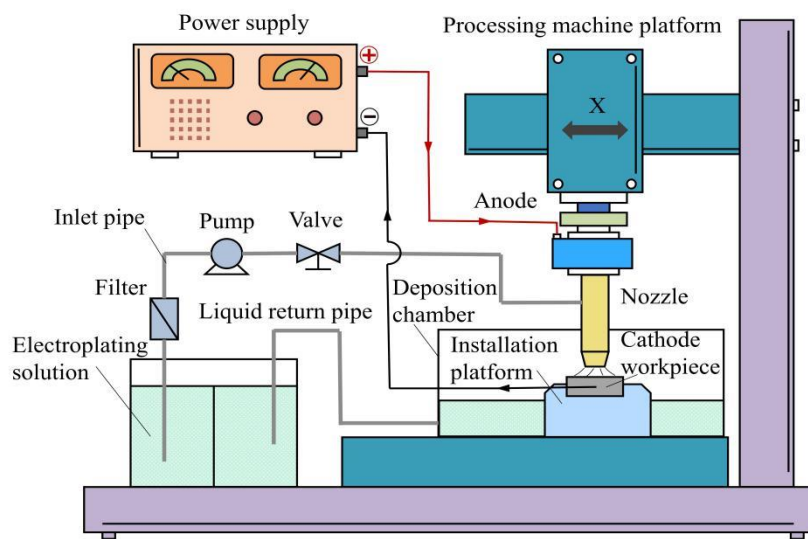


Figure 1. Schematic configuration of the electric spraying test

Table 1. Chemical composition of the plating solution

Composition	Content/(g·L ⁻¹)
NiSO ₄ ·6H ₂ O	200
NiCl ₂ ·6H ₂ O	30
H ₃ PO ₃	20
H ₃ BO ₃	30
C ₆ H ₈ O ₇	60
CH ₄ N ₂ S	0.01
C ₁₂ H ₂₅ SO ₄ Na	0.08
La ₂ O ₃	2.5

2.2 Test instruments

In this section, scanning electron microscopy (Quanta FEG250; FEI Instrument Co., Oregon, USA) was utilized to observe the surface morphology of the coating and wear marks. Accordingly, the surface roughness and flatness of the coating were studied. Moreover, chemical composition of the coating was analyzed by an EDS analyzer (XFlash 5030 Bruker AXS, Inc., Berlin, Germany) to determine the best chemical composition of the coating and the scanning method. Microhardness tester

(Duramin - 40; Struhrs, Denmark) was applied to measure the microhardness of the coating surface. In the experiment, the test load and the load duration were set to 100g and 15s, respectively. Five values were measured and the average was considered as the test result. A comprehensive performance tester was applied to detect the surface wear-resistance of the coating. During the test, the instrument moved along a straight line for 20 min, while the reciprocating speed, grinding crack length and load were set to 500 T/min, 4 mm and 320 g, respectively. A laser confocal microscope (OLYMPUS LEXT4100, OLYMPUS Corporation, Japan) was used to measure the dimensional parameters, including width, depth and section area, of the surface wear of the coating. It is worth noting that these dimensions will be utilized to evaluate the wear-resisting properties of the material according to the dimension of the attrition mark. Electrochemical workstation (CS350, Co name, Country of origin) was used to measure the polarization curve and impedance spectrum. In the experiment, 35% NaCl solution was used as the corrosive medium. This solution is similar to the seawater that corrodes the coating on the workpiece surface and it is the most common corrosive solution in practical applications. During the test, only 1 cm² of the workpiece was in contact with the corrosive liquid, while the rest of the surface was covered by an epoxy resin. The corrosion processes for open circuit potential, potentiodynamic scanning and AC impedance are conducted for 3 to 4 hours.

3. RESULTS AND DISCUSSION

3.1 Surface microstructure analysis of the coating layer

Figure 2 shows the surface microstructure of the composite coating under different current densities. It is found that typical crystal cell structures appear on the coating surface. This phenomenon originates from the diffusion of Ni and P molecules of the coating surface into the solid solution under the induction of the catalytic active center, thereby forming a crystal cell structure [21]. It should be indicated that this formation follows the two-dimensional growth model for the crystal nucleus [22]. When the current density is set to 16 A/dm², the composite coating has an obvious concave and convex surface, uneven distribution of particles on the coating, and a surface with holes forms. Moreover, it is found that as the current density increases, the coating surface has obvious improvement. When the current density approaches 32 A/dm², the coating surface microstructure is optimized, the pit bump phenomenon largely disappears and a close connection forms between cell surfaces so that a uniform size distribution is obtained. As the current density increase, the surface microstructure of the coating begins to deteriorate, and when the current density approaches 48 A/dm², the surface becomes uneven. In this case, the cell size is not uniform and pores appear on the cell.

Performed analysis shows that when the current density is small, an ion deposition in the order of only a few nanometers forms in the coating surface. Meanwhile, when the nucleation rate is low, xxx cannot satisfy the dispersion strengthening and fine grain strengthening effect. As the current density and deposition rate rise quickly, grain refining makes the uniform surface cell structure fine. On the other hand, when the current density is too high, the deposition process of particles is inhibited and the transfer of nano-ions in the electroplating solution is controlled by the ultrasonic forced convection [23]. This relatively decreases the presence of lanthanum particles in the composite coating, which affects the dispersion strengthening and grain refining effect of particles.

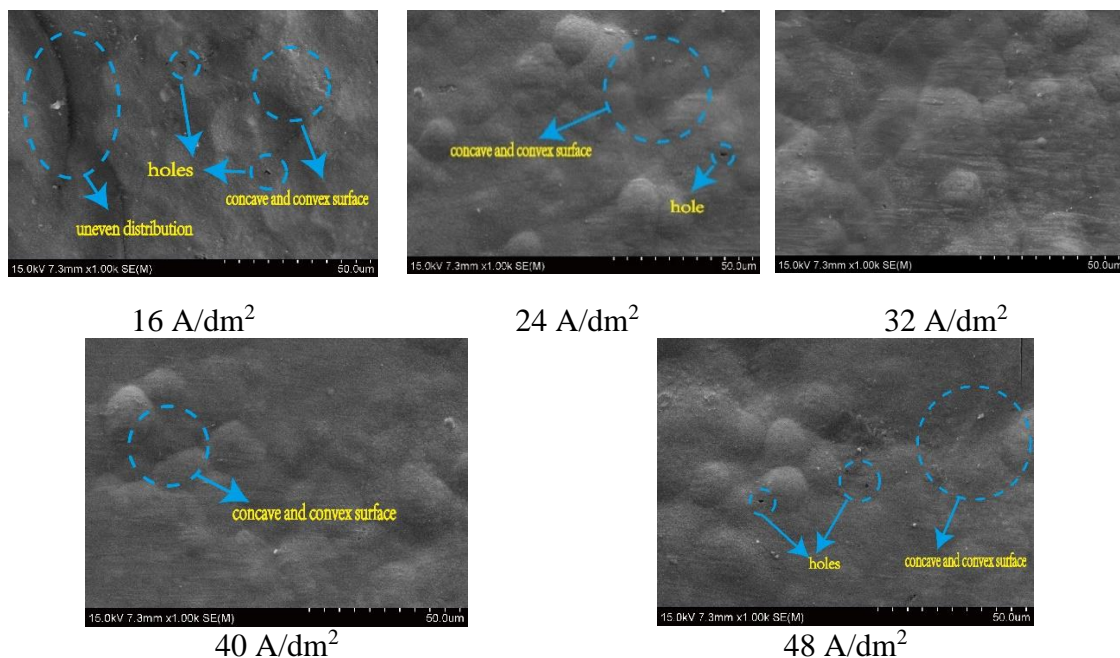


Figure 2. Surface micromorphologies of Ni-P-La₂O₃ composite coatings prepared at different current densities.

3.2 Element content analysis of coating

Table 2 and Figure 3 show the surface element mass fraction and EDS spectrum of each element in the composite coating, respectively. Since the table data can be obtained at different current densities, the mass fraction of each element receives the influence of different levels. When the current density approaches 16 A/dm², the mass fraction of Ni, P and La elements approach 93.83%, 4.69% and 1.49%, respectively. Moreover, it is found that when the current density approaches 32 A/dm², mass fractions of Ni, P and La elements approach 91.89%, 5.37% and 2.74%, respectively. For current densities higher than 32 A/dm², the mass fraction of Ni element increases, while those of P and La elements reduce. Accordingly, it is found that the mass fraction of Ni element initially decreases and then increases, while the mass fraction of the other two elements has an opposite trend. Based on the performed analysis, it is concluded that the increase of the current density is conducive to the polarization reaction of the cathode, resulting in a remarkable La₂O₃ deposit on the coating surface. Lanthanum, as a most abundant rare-earth element, has an effective charge and strong adsorption capacity, which can make the charge move faster. When the current density is too high, the cathode reaction rate will be too high so that some elements cannot be absorbed by the coating surface. Consequently, the element mass fraction changes again.

It is concluded that when the current density is small, the cathode polarization effect is weak and nanoparticles do not deposit so that the deposition rate is low. Therefore, only a small amount of nano-ion deposition forms on the coating surface. It is observed that as the current density increases, the cathode polarization effect strengthens and a large amount of nano-particles deposits on the coating surface. Meanwhile, the mass fraction of La element relatively rises. However, when the current density

is too large, the reunion phenomenon happens, which leads to difficult deposition on the workpiece surface. In the conducted experiment, La_2O_3 reunion falls off from the coating surface, which reduces the quality score [24].

Table 2. Mass fraction of elements in the coating surface prepared by different current densities.

Current density (A/dm^2)	Ni (%)	P (%)	La (%)
16	93.83	4.69	1.49
24	93.24	4.9	1.94
32	91.89	5.37	2.74
40	93.06	4.58	2.37
48	94.73	3.43	1.82

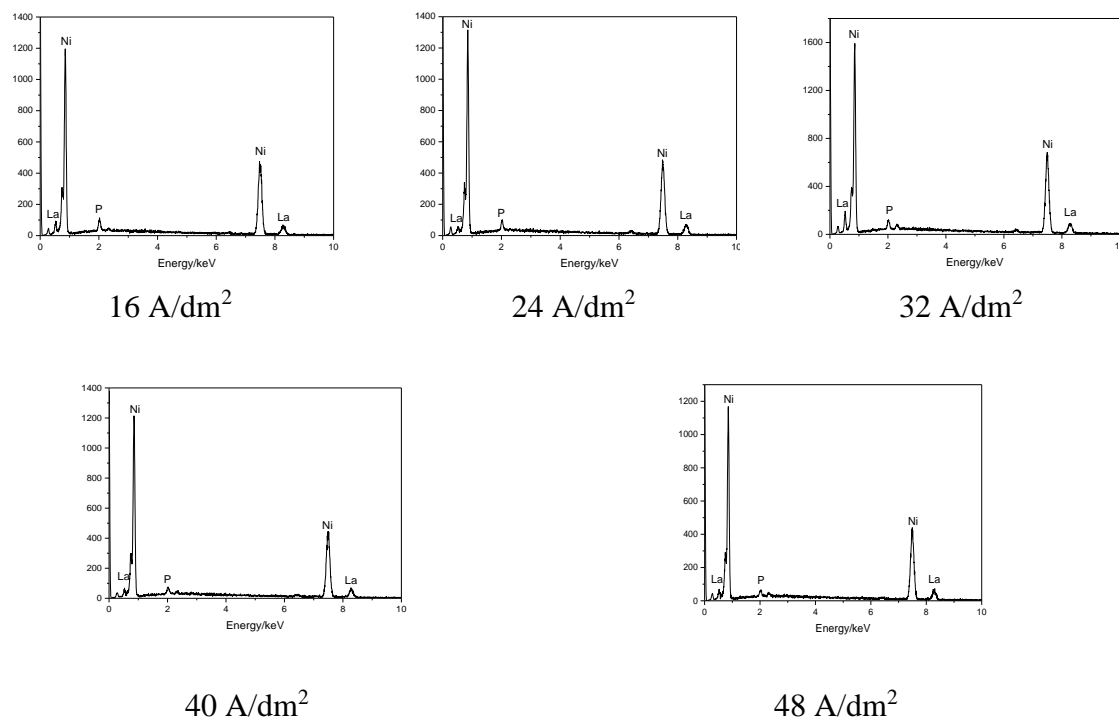


Figure 3. EDS spectra of Ni-P- La_2O_3 composite coatings prepared at different current densities.

3.3 Microhardness analysis of the coating

Figure 4 shows the microhardness of the coating for different current densities. It is observed that the hardness initially increases and then decreases. Moreover, as the current density increases from $16 \text{ A}/\text{dm}^2$ to $32 \text{ A}/\text{dm}^2$, the microhardness of the coatings increases from $585.94 \text{ HV}_{0.1}$ to $822.83 \text{ HV}_{0.1}$. When the current density is low, electrostatic attraction of lanthanum oxide (La_2O_3) forms a relatively weak cathode. Moreover, the ion deposition rate in the plating solution is low. Therefore, the coating rate

of nanoparticles is relatively low and the microhardness of the coating is low. When the current density reaches 32 A/dm^2 , the deposition rate of La_2O_3 nanoparticles reaches the maximum. La_2O_3 nanoparticle, as a hard and strong phase distributed in the coating, can strengthen the dispersion and hinder the deformation of the coating, thereby improving the hardness of the coating [25]. As the current density increases from 32 A/dm^2 to 48 A/dm^2 , the microhardness of the coating decreases from $822.83 \text{ HV}_{0.1}$ to $567.88 \text{ HV}_{0.1}$. This may be attributed to the high current density and strong reaction. It is found that nanometer ions that deposit shortly after the initial deposition are unable to adhere to the surface of the coating with the flushing of the plating solution. Therefore, the ion adhesion on the surface of the coating significantly reduces, thereby affecting the improvement of the coating hardness [26].

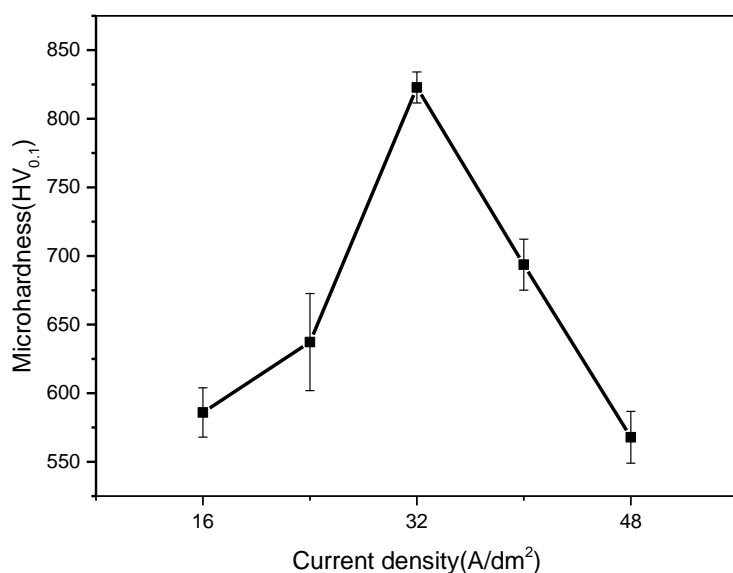


Figure 4. Microhardness on the coating surface, prepared by different current densities

3.4 Analysis of the wear resistance of the coating

Figure 5 presents the abrasion scars on the surface of the coating obtained from different current densities, obtained from the friction of the GCr15 grinding ball. Table 3 shows the cross-section parameters given by the laser confocal microscope after wear. The composite coating by the grinding ball wear shows obvious wear marks, resulting in the plastic deformation of the coating. The surface hardness in the plastic deformation area is too low so that the coating can be easily cracked and fractured. When the current density increases from 16 A/dm^2 to 48 A/dm^2 , the width, height and section area of the wear marks initially decreases and then increases. It is found that as the current density increases from 16 A/dm^2 to 32 A/dm^2 , the coating abrasion resistance improves, the wear mark gradually becomes straight and the wear scar becomes shallow. Moreover, as the current density increases from 32 A/dm^2 to 48 A/dm^2 , the coating wear resistance decreases, abrasion marks sag degree becomes more obvious, and the scar deepens. When the current density is set to 32 A/dm^2 , the best coating wear-resisting performance is obtained. Moreover, it is found that the grinding crack width and height in the cross-section area of $2264.829 \mu\text{m}^2$ are $448.125 \mu\text{m}$ and $6.897 \mu\text{m}$, respectively.

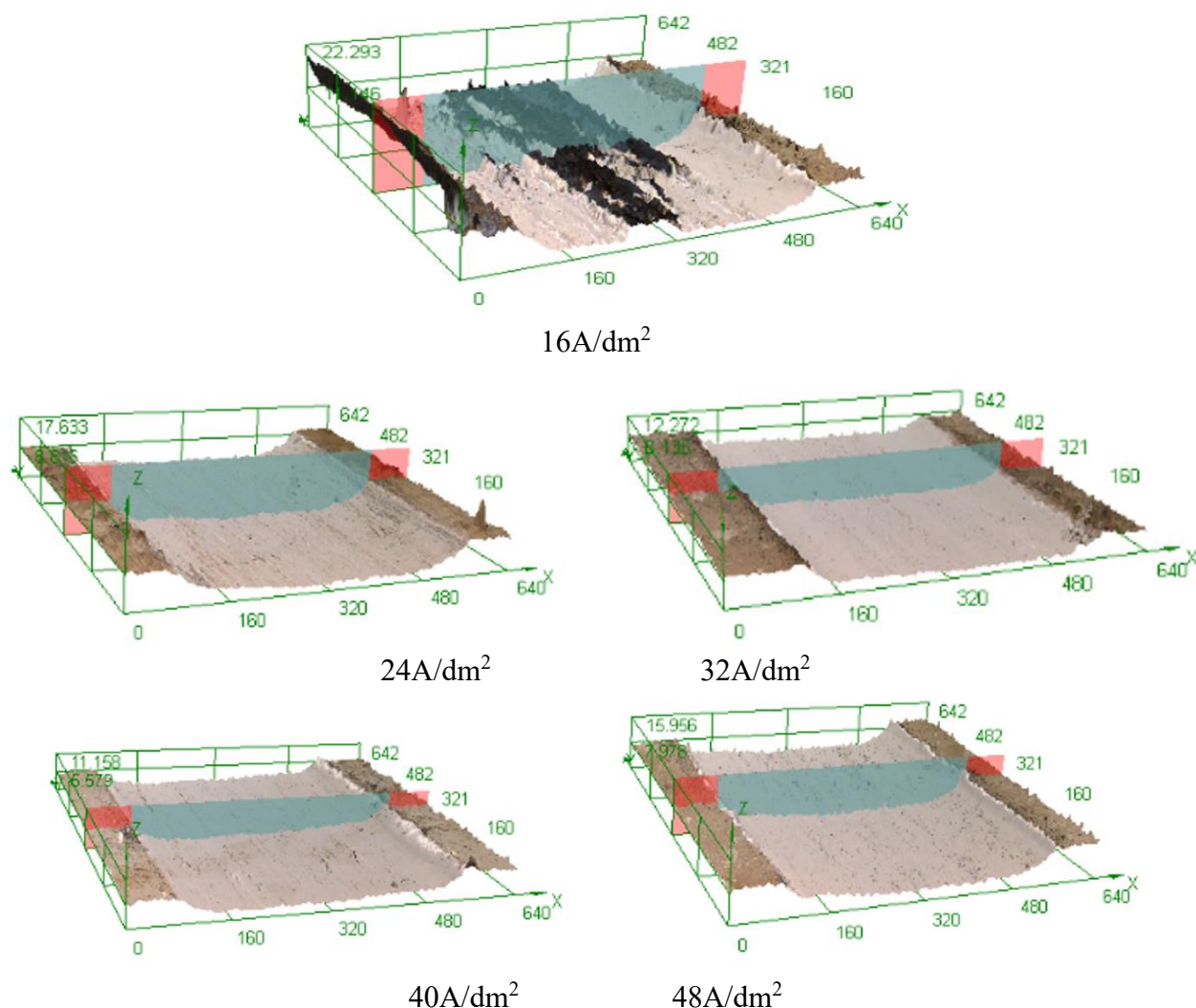


Figure 5. Cross-section morphology of the composite coating prepared by different current densities after GCr15 grinding ball wear

Table 3. Wear scar cross-section parameters of the composite coating prepared with different current densities after wear.

Current density (A/dm ²)	Width (μm)	Height (μm)	Scratch area (μm ²)
16	493.750	12.183	3943.550
24	476.875	09.125	3174.122
32	448.125	06.897	2264.829
40	470.625	07.709	2692.186
48	483.125	11.961	3352.984

Figure 6 shows the scars produced by friction on the composite coating surface, which are analyzed by the scanning electron microscope. According to the analysis carried out by the scanning electron microscope, it is found that scars on the composite coating surface are correlated with the current density. As the current density increases, the surface scars initially flatten and then become rough [27].

When the current density is low, there are few surface coatings and nanoparticles on the surface to form an effective hard layer on the surface of the coating. The continuous friction of the steel ball causes the surface of the coating to heat and soften. Therefore, the surface of the coating becomes uneven locally agglomerated. Moreover, black Fe appears on the coating surface. It should be indicated that the friction mechanism is particle wear and surface fatigue wear. When the current density increases, the nanoparticles can be fully deposited on the surface of the coating. The nanoparticles are uniformly distributed on the surface of the coating, thereby playing a good dispersion effect on the surface and forming an effective hard layer on the surface. Therefore, the wear resistance of the coating surface is significantly improved. As the current continues to increase, cracks and surface peeling appear, and the wear marks on the coating surface are more obvious, which worsens the wear resistance of the coating surface [28,29].

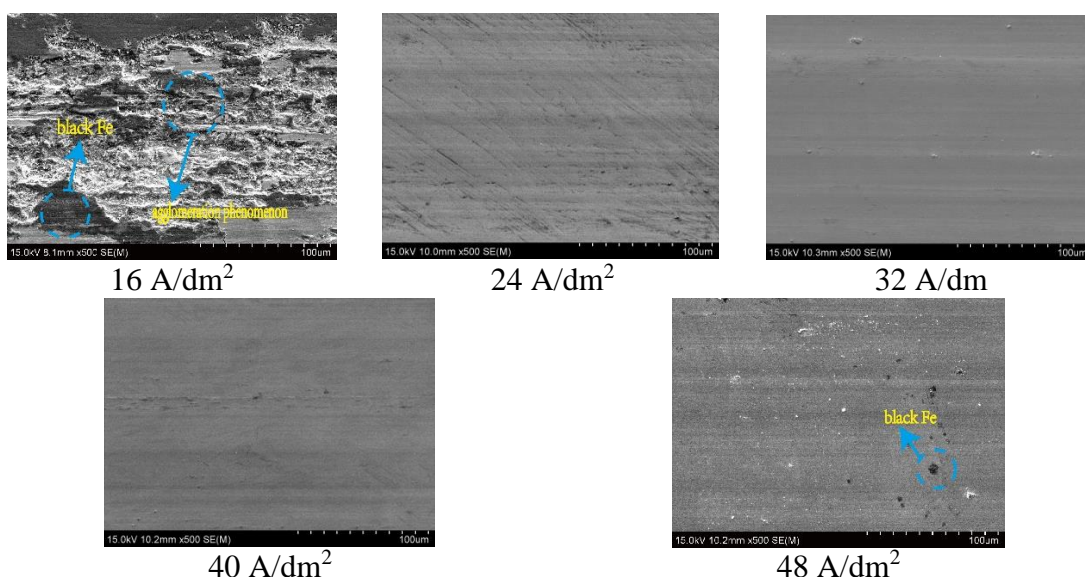


Figure 6. SEM images of wear scars of composite coatings prepared with different current densities after wear.

The analysis shows that there is a positive correlation between wear resistance and hardness and both of them achieve the best effect when the current density is $32 \text{ A}/\text{dm}^2$.

When the highest hardness, coating the surface of the deposition of nanoparticles, nanoparticles at this time as the hard layer of uniform density distribution in the coating surface, to protect the role of composite coating, while the grinding crack morphology is the best, the grinding crack depth, width, have reached the minimum cross-section area, the nail-pierced effect of nano ions to further improve, in the coating surface forming a layer of abrasion resistance box. When the current density is too high, the surface quality of the coating and the hardness decrease. Moreover, the surface appearance of the wear marks becomes obviously rough, and the wear resistance of the coating decreases. Therefore, when the micro-hardness of the coating surface is higher, the wear resistance improves significantly.

3.5 Corrosion resistance analysis of the coating

3.5.1 Analysis of the composite coating polarization curve

The polarization curve and corrosion resistance parameters of the composite coating under different current densities are obtained using the Cview software and polarization curve epitaxy method. Figure 7 and Table 4 show that the self-corrosion current density and the self-corrosion potential have an opposite correlation. The lower the self-corrosion current density, the higher the self-corrosion potential, and the better the corrosion resistance of the composite coating. When the current density is $16 \text{ A}/\text{dm}^2$, the self-etching current density is $1.46\text{E-}5 \text{ A}\cdot\text{cm}^{-2}$, which is the highest among all self-etching current densities. Moreover, the corresponding self-etching potential is -0.461V , and the corrosion potential reaches the minimum value. When the current density increases to $32 \text{ A}/\text{dm}^2$, the self-etching current density reaches the minimum value of $5.61\text{E-}7 \text{ A}\cdot\text{cm}^{-2}$, the self-etching potential reaches -0.197V , and the corrosion resistance of the composite coating reaches the best. When the current density is $32 \text{ A}/\text{dm}^2$, the self-etching potential increases by 59.2% and the self-etching current density decreases by 96.2% compared with that of the current density of $16 \text{ A}/\text{dm}^2$. The current density and the self-etching current density continue to increase. According to the data in the table, the corrosion resistance of the coating initially increases and then decreases as the current density increases.

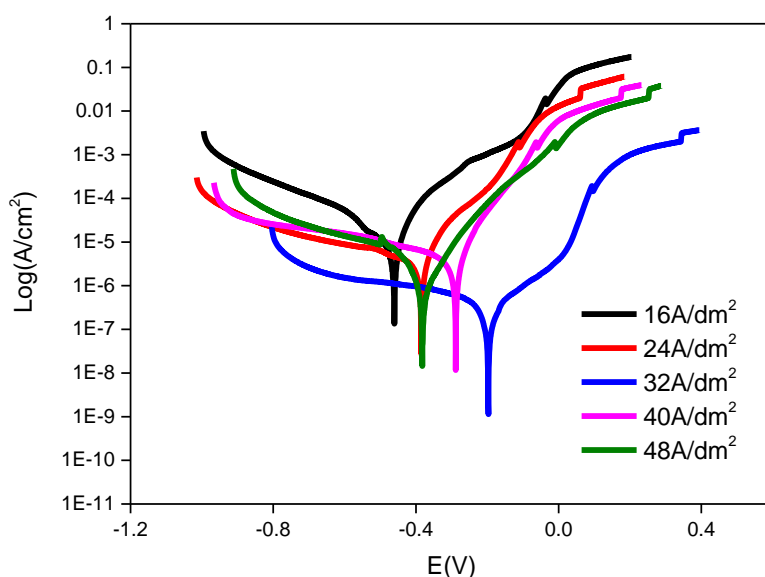


Figure 7. Potentiodynamic polarization curves of Ni-P-La₂O₃ nanocomposite coatings prepared by jet electrodeposition under different machining gaps obtained by corrosion tests at a scanning rate of 1 mV/s in 3.5 wt.% NaCl solution.

The results show that the surface material of the composite coating changes as the current density changes. When the current density is low, the coating on the surface of the rare earth element La is relatively small and cannot be formed on the surface of a coating for protection. Although the Ni-P coating can form a layer of the protective film, the coating surface is not complete. Considering low electrode potential, corrosion from Ni-P coating cracks begin to corrosion of artifacts, can alleviate the

corrosion process, while the effect not beautiful [30]. As the current density increases, the relative content of nanocrystalline ions increases, which enhances the fine crystal on the surface of the coating, and the defects such as cracks on the surface of the coating decrease [31]. Meanwhile, the corrosion circuit with the grain boundary as the anode and the crystal lattice as the cathode is blocked. Therefore, the corrosion progress further slows down. When the current density is too high, the reaction is intensive and the surface adsorption of nano-ions is inhibited. Therefore, a large number of particles become granular and cannot be fixed on the surface of the coating. Moreover, the surface of the coating becomes rough, the fine crystals weaken. Furthermore, the corrosion reaction intensifies, thereby reducing the corrosion resistance of the coating [32,33].

Table 4. Parameter values of the polarization curve.

Current density (A/dm ²)	E_{corr} (V)	I_{corr} (A·cm ⁻²)	Corrosion rate (mm/a)
16	-0.461	1.46E-5	0.1765
24	-0.385	2.00E-6	0.0870
32	-0.197	5.61E-7	0.0068
40	-0.288	5.90E-6	0.0714
48	-0.382	2.00E-6	0.0243

3.5.2 Electrochemical Impedance curve analysis

The Nview software is utilized to test the alternating impedance of the coating. Moreover, Figure 8 and Table 5 illustrate the Nyquist plots of the Ni-P- La₂O₃ composite coating, the fitted equivalent circuit and the equivalent circuit parameters, respectively. It should be indicated that R_s, R_p and CPE are the solution resistance, charge transfer resistance and constant phase angle element, respectively. The corrosion resistance of the composite coating is reflected by the radius of the capacitive reactance arc. The higher the radius of the capacitive reactance arc is, the better the corrosion resistance of the composite coating is. Figure 8 shows that as the current density increases, the capacitive reactance arc radius of rendering initially increases and then decreases. It is found that the maximum capacitive reactance arc radius is obtained when the current density is set to 32 A/dm². Meanwhile, the maximum charge transfer resistance is 18128 Ω·cm⁻². It indicates that the bigger the corrosion, the slower it is. The comparison with the polarization curve shows that the obtained results are consistent, and the corrosion resistance is the best when the current density is 32 A/dm² [34].

The performed analysis demonstrates that when the current density is small, the concentration of La₂O₃ in the surface coating reduces, and defects of the coating surface increases. On the other hand, as the current density increases, La₂O₃ content increases and the composite coating of fine-grain strengthening effect improves. Accordingly, the coating surface becomes more even and defects reduce. It should be indicated that when the current density is too large, nanoparticles cannot deposit on the surface coating so that La₂O₃ content reduces. Consequently, the reinforcement effect of the composite coating and the corrosion resistance reduces. According to the tests of the potentiometric polarization

curve and electrochemical impedance spectrum curve, the Ni-P-La₂O₃ deposit can improve the corrosion resistance of the workpiece surface under different current densities.

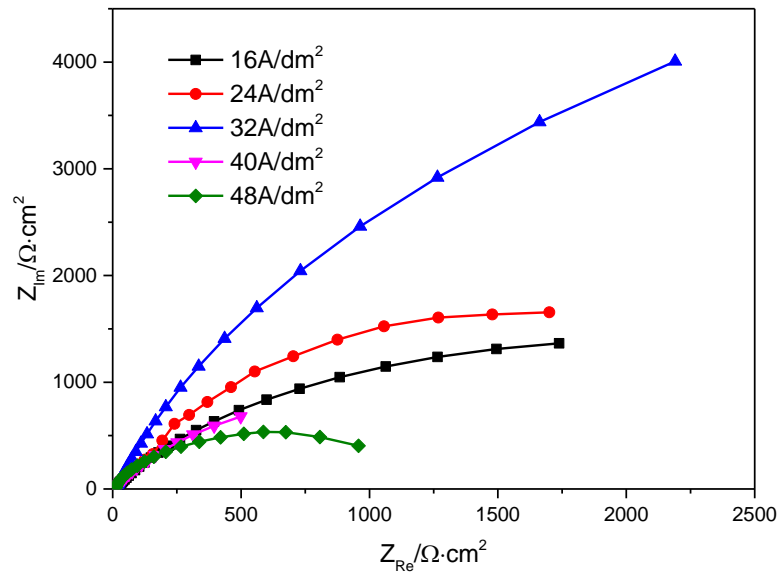


Figure 8. EIS curves of Ni-P-La₂O₃ nanocomposite coatings prepared by jet electrodeposition under different machining gaps obtained by corrosion tests at a scanning rate of 1 mV/s in 3.5 wt.% NaCl solution.

Table 5. Equivalent circuit parameter values.

Current density (A/dm ²)	R _s (Ω·cm ⁻²)	CPE-T (F·cm ⁻²)	CPE-P	R _p (Ω·cm ⁻²)
16	6.58	7.96E-5	0.733	4534
24	9.07	5.85E-3	0.764	4747
32	9.63	3.35E-5	0.853	18128
40	10.50	9.59E-3	0.816	2235
48	8.39	1.12E-2	0.904	1141

3.5.3 Surface morphology analysis of the composite coating after corrosion

Figure 9 shows the effect of Ni-P- La₂O₃ composite coating on the surface morphology after corrosion. The SEM analysis shows that when the current density is 16 A/dm², the coating surface is uneven, and there are many cracks and corrosion products. As the current density increases, the corrosion morphology improves and no concave and convex surface is observed. Moreover, when the current density is 32 A/dm², the corrosion morphology obtains the best condition. It is observed that when the current density is low, the nanometer ion plating quantity is less and a large number of holes appear on the surface of the coating. When the corrosion reaction occurs, the corrosive particles directly pass

through the holes to corrode the surface. As the current density increases, the surface of the nano-ions forms a hard layer on the coating surface. In this case, the surface coating plays a buffer role [35]. Moreover, during the corrosion process, Ni-P and nano ions form corrosion batteries, which effectively inhibit the corrosion process. When the current density is too high, the surface quality of the coating deteriorates and many defects are found, which aggravate the corrosion reaction and cause serious surface corrosion. Moreover, a large number of cracks appear.

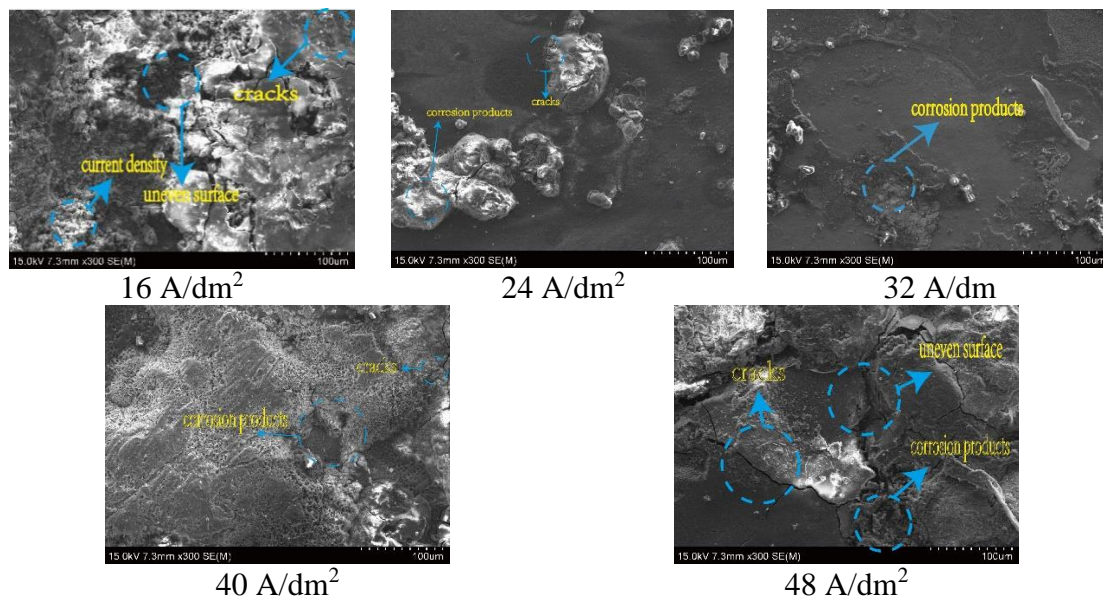


Figure 9. Corrosion morphology of Ni-P-La₂O₃ nanocomposite coatings prepared by jet electrodeposition under different machining gaps obtained by corrosion tests at a scanning rate of 1 mV/s in 3.5 wt.% NaCl solution.

4. CONCLUSIONS

The following conclusions are drawn from the present study:

The Ni-P-La₂O₃ composite coating prepared by the jet electrodeposition presents a typical cell structure. Moreover, the surface morphology of the coating changes as the current density changes. It is found that as the current density increases, the surface quality initially increases and then decreases. When the current density reaches 32 A/dm², the coating surface quality is the best. Moreover, cells are connected closely with uniform distribution.

During the increment of the current density of the Ni-P-La₂O₃ composite coating, the mass fraction of surface elements changes. The mass fraction of Ni elements initially decreases and then increases, while the mass fraction of P and La elements initially increases and then decreases. When the current density is 32 A/dm², the mass fraction of the La element reaches the maximum value.

The microhardness of the Ni-P-La₂O₃ composite coating initially increases and then decreases. When the current density is 32 A/dm², the microhardness of the coating surface reaches 822.83HV_{0.1},

which is about 45% higher than that when the current density is $48\text{A}/\text{dm}^2$. Meanwhile, the microhardness of the composite coating reaches the highest value.

The wear resistance of the Ni-P-La₂O₃ composite coating initially increases and then decreases as the current density increases up to $32\text{ A}/\text{dm}^2$, coating the surface of the grinding crack width, depth and area. evenly distributed in the coating on the surface of nanoparticles, the surface has played a very good dispersion effect, formed on the surface of the hard layer, have the effect of the protective film on the surface of a coating, at this point, the wear resistance of the coating in the best.

The corrosion resistance of the Ni-P-La₂O₃ composite coating initially increases and then decreases as the current density increases. When the current density is $32\text{A}/\text{dm}^2$, the minimum self-etching current density and the maximum self-etching potential are $5.6099\text{E-7}\text{A}\cdot\text{cm}^{-2}$ and -0.19702V , respectively. Moreover, the charge transfer resistance and the capacitance-arc are the maximum. Furthermore, the corrosion resistance of the coating surface is the lowest and the corrosion resistance reaches the optimum value.

ACKNOWLEDGMENTS

Financial support for this work was provided by the Fundamental Research Funds for the Central Universities (Grant number KYXJ202002), the National Natural Science Foundation of China (Grant number 31901455), the Natural Science Foundation of Jiangsu (Grant number SBK2018041878), the Postdoctoral fund of China (Grant number 2018M632314), Nanjing Agricultural University Innovation Training Plan (Grant number 202030XX42), Innovation Training Plan for College Students of Jiangsu (Grant number 202010307154Y).

References

1. X. Q. Fu, M. Q. Shen, J. R. Lin, X. S. Wang, Q. Q. Wang, Y. Xu, *Int. J. Electrochem. Sci.*, 15(2020)816-829.
2. W. Jiang, L. D. Shen, K. Wang, Z. W. Wang, Z. J. Tian, *Proc. Inst. Mech. Eng. J. Eng. Manuf.*, 234(2020)431-438.
3. L. L. Ji, F. D. Chen, H. Huang, X. Y. Sun, Y. Y. Yan, X. B. Tian, *Surf. Coat. Technology*, 351(2018)212-219.
4. J. Tan, H. Song, X. H. Zheng, Q. Zhang, M. Wang, *Surf. Eng.*, 34(2018)861-869.
5. F. F. Xia, W. C. Jia, M. Z. Jiang, W. Cui, J. Wang, *Ceram. Int.*, 43(2017)14623-14628.
6. W. Jiang, L. D. Shen, M. Y. Xu, Z. W. Wang, Z. J. Tian, *J. Alloys Compd.*, 791(2019)847-855.
7. Q. Zhang, J. Tian, L. D. Meng, F. K. Xie, H. C. Zhao, Z. Yan, *Applied. Sciences, Basel*, 9(2019)24.
8. M. Q. Shen, X. Q. Fu, X. S. Wang, J. R. Lin, Q. Q. Wang, *Nanosci. Nanotechnol. Lett.*, 11(2019)938-946.
9. W. Jiang, L. D. Shen, M. B. Qiu, M. Y. Xu, Z. J. Tian, *Mater. Res. Express.*, 5(2018)9.
10. W. Cui, K. Wang, F. F. Xia, P. Wang, *Ceram. Int.*, 44(2018)5500-5505.
11. Y. H. Wang, L. D. Shen, M. B. Qiu, Z. J. Tian, X. Liu, W. Zhuo, *J. Electrochem. Soc.*, 163(2016)D579-D584.
12. J. S. Chen, Y. H. Huang, C. Z. Wei, B. Q, J. M. Yang, Y. Q. He, *Advanced. Composites. Letters*, 19(2010)184-188.
13. H. Fan, Y. P. Zhao, S. K. Wang, H. F. Guo, *Int. J. Adv. Manuf. Technol.*, 105(2019)4509-4516.
14. W. B. Lu, X. F. Cui, G. Jin, M. L. Dong, Y. C. Fang, X. Wen, W. Y. Ma, *Opt. Laser. Technol.*, 129(2020).

15. M. Q. Shen, X. Q. Fu, S. L. Duan, Q. Q. Wang, Y. Xu, W. K. Ma, *Mater. Sci. Technol.*, (2020), (in Chinese).
16. Y. L. Wang, D. J. Shen, B. Liao, *Mater. Prot.*, (2002)41-42, (in Chinese).
17. M. A. A. Taib, Z. D. I. Sktani, N. A. Rejab, K. C. Xian, Z. A. Ahmad, *Mater. Today: Proc.*, 17(2019)1086-1092.
18. A. Guha, A. Basu, *J. Fluoresc.*, 24(2014)683-687.
19. D. D. Gu, Y. F. Shen, *J. Phys. Appl. Phys.*, 41(2008).
20. S. A. Zhou, W. P. Jia, W. R. Chen, *Electroplat. Pollut. Control.*, 40(2020)7-10, (in Chinese).
21. X. Q. Fu, S. L. Duan, J. R. Lin, M. Q. Shen, Q. Q. Wang, *Rare. Met. Mater. Eng.*, 49(2020)2095-2103, (in Chinese).
22. E. Beltowska. Lehman, P. Indyka, A. Bigos, M. J. Szczerba, M. Kot, *Mater. Des.*, 80(2015)1-11.
23. F. C. Walsh, C. T. J. Low, J. O. Bello, *Trans. IMF*, 93(2015)147-156.
24. X. H. Dou, *Rare. Reath. Inf.*, (2005)33-34, (in Chinese).
25. H. C. Lin, *Shanghai Nonferrous Met.*, (2007)196-200, (in Chinese).
26. L. Hui, Z. He-Ling, *Plat. Surf. Finish.*, 91(2004)66-69.
27. C. S. Liu, D. D. Wei, X. Y. Huang, Y. J. Mai, L. Y. Zhang, X. H. Jie, *J.Mater. Res.*, 34(2019)1726-1733.
28. V. V. N. Reddy, B. Ramamoorthy, P. K. Nair, *Wear.*, 239(2000)111-116.
29. Y. C. Wu, G. H. Li, L. Zhang, *Surf. Eng.*, 16(2000)506-510.
30. Prasanna. Gadhari, Prasanta. Sahoo, *Prot. Electrochim. Acta*, 33(2015)49-68.
31. Prasanna. Gadhari, Prasanta. Sahoo, *Prot. Electrochim. Acta*, 32(2014)137-156.
32. S. Sadreddini, A. Afshar, *Appl. Surf. Sci.*, 303(2014)125-130.
33. J. Kubisztal, J. Niedbala, A. Budniok, *Surf. Interface Anal.*, 42(2010)1222-1225.
34. J. N. Balaraju, T. S. N. S. Narayanan, S. K. Seshadri, *J. Solid. State. Electrochem.*, 5(2001)334-338.
35. S. A. Lajevardi, T. Shahrabi, *Appl. Surf. Sci.*, 256(2010)6775-6781.

© 2020 The Authors. Published by ESG (www.electrochemsci.org). This article is an open access article distributed under the terms and conditions of the Creative Commons Attribution license (<http://creativecommons.org/licenses/by/4.0/>).